# Manipulating counter-rotating interactions in the quantum Rabi model via modulation of the transition frequency of the two-level system

Jin-Feng Huang, Jie-Qiao Liao, Lin Tian, and Le-Man Kuang

Phys. Rev. A **96**, 043849 — Published 20 October 2017

DOI: 10.1103/PhysRevA.96.043849

# Manipulating counter-rotating interactions in the quantum Rabi model via modulating the transition frequency of the two-level system

Jin-Feng Huang,[1,2,*] Jie-Qiao Liao,[1,2,†] Lin Tian,[2] and Le-Man Kuang[1]

[1] *Key Laboratory of Low-Dimensional Quantum Structures and Quantum Control of Ministry of Education, Department of Physics and Synergetic Innovation Center for Quantum Effects and Applications, Hunan Normal University, Changsha 410081, China*

[2] *School of Natural Sciences, University of California, Merced, California 95343, USA*

(Dated: October 5, 2017)

We propose a theoretical approach to manipulate the counter-rotating (CR) interactions in the quantum Rabi model by introducing a sinusoidal modulation to the transition frequency of the quantum two-level system. By choosing appropriate modulation frequency and amplitude, enhancement and suppression of the CR interactions can be achieved in the Jaynes-Cummings regime (including both weak- and strong-coupling cases) as well as the ultrastrong-coupling regime. In particular, we calculate the output excitation emission of the bosonic vacuum state under enhanced CR terms. Our results show that continuous and steady bosonic excitation emission from the bosonic vacuum can be observed in the Jaynes-Cummings regime as a consequence of the enhancement. Our approach is general and system-independent, and hence it works for various physical systems described by the quantum Rabi model. As an example, we discuss the implementation of this scheme with superconducting quantum circuits.

PACS numbers: 42.50.Pq, 42.50.Dv

## I. INTRODUCTION

The quantum Rabi model [1, 2], one of the fundamental models in quantum optics, describes the interaction between a quantum two-level system (natural or artificial atom, qubit) and a bosonic mode (optical mode, microwave mode). Based on the coupling strength between the two-level system and the bosonic mode, the quantum Rabi model possesses two important parameter regimes. For an interaction strength much smaller than the frequencies of the two-level system and the bosonic mode (which are near resonance), the quantum Rabi Hamiltonian can be reduced to the Jaynes-Cummings (JC) Hamiltonian [3, 4] under the rotating-wave approximation (RWA), i.e., the counter-rotating (CR) terms in the interaction can be omitted, and the model can be solved analytically with simple functions. This is the so-called JC regime, which can be further divided into weak- and strong-coupling regimes [5]. Cavity-QED systems formed by natural atoms coupled to optical cavities are well within this regime, which makes the JC model one of the most significant models in quantum optics. The other interesting regime is the ultrastrong-coupling regime, where the light-matter coupling strength reaches a considerable fraction of the frequencies of the two-level system and the bosonic mode. In this regime, the RWA is no longer valid, and the CR interactions strongly modify the eigenenergies of the JC model [6–8]. To date, the ultrastrong-coupling regime has been demonstrated in superconducting circuits [9–13] and semiconductor microcavities [14–16], with coupling strengths exceeding 10% of the resonance frequencies of the two-level system or the bosonic mode. Moreover, the ultrastrong-coupling regime can be simulated with various cavity-QED [17] and circuit-QED [18] systems. Recently, even the deep-strong-coupling regime has been reported, with a coupling strength comparable or larger than the two-level system or the resonator frequency [12].

In the past few years, enormous effort has been devoted to the study of the ultrastrong-coupling regime in the quantum Rabi model, and great advances have been achieved in both experimental and theoretical aspects. For example, it was found that the CR terms can induce novel quantum phenomena: such as asymmetry of the vacuum Rabi-splitting [19], virtual-photon-induced vacuum Rabi oscillation [20], superradiance transition [21], non-classical photon statistics [22, 23], spontaneous release of virtual photons [24, 25], parity-dependent state engineering [26], and multi-photon sideband transitions [27]. Moreover, interesting quantum dynamical phenomena have been reported, such as collapse and revival of quantum states [28], quantum Zeno and anti-Zeno effects [29, 30], single-photon scattering [31, 32], collective spontaneous emission in multi-atom systems [33–35], and multiphoton quantum Rabi oscillations [36].

It should be mentioned that, though the coupled Rabi system exhibits some interesting quantum phenomena in the ultrastrong-coupling regime, it also brings some undesired quantum effects for some particular tasks. For example, in some quantum information processing tasks demanding excitation conservation such as quantum state transfer, it is desired to suppress the CR interaction terms because these terms will lead to undesired transitions changing the excitations of the system two by two. On the other hand, the CR interaction terms are very

* jfhuang@hunnu.edu.cn
† jqliao@hunnu.edu.cn

useful in some tasks because these terms can be used to create quantum entanglement involving photons and atoms in some cavity-QED systems in a manner of simultaneously exciting atom and photon. Therefore, the manipulation of the CR terms and the rotating terms is a key technique in coupled atom-cavity field systems. In this way, the quantum effects associated with the CR terms can be enhanced or suppressed on demand [37]. In the weak- or strong-coupling regime, manipulating the CR interactions can help us observe some quantum effects induced by CR terms; whereas in the ultrastrong-coupling regime, these techniques can help us to suppress the effects caused by CR terms, and then the system recovers the JC dynamics. Recently, Liberato *et al.* proposed a method to enhance the processes by CR interactions, which requires the coupling strength to oscillate at twice the frequency of the cavity mode [38]. Huang and Law proposed a scheme to control the CR interactions using a sequence of phase kicks [37].

In this paper, we propose a theoretical approach to manipulate the interactions between the quantum two-level system and the bosonic mode in the quantum Rabi model by introducing a monochromatic modulation of the transition frequency of the two-level system. This frequency modulation induces a series of sidebands in the spectrum of the quantum two-level system, and affects the detunings between the two-level system and the bosonic mode. By engineering appropriate modulation frequency and amplitude, the detunings and the effective coupling strengths between the two-level system and the bosonic mode can be controlled to make desired transitions on resonance and undesired transitions far off-resonance. With this approach, we can enhance the CR interactions in the JC regime, and suppress the CR interactions in the ultrastrong-coupling regime. We also show that in the JC regime, the enhanced CR interactions can induce stronger bosonic excitation emission from bosonic vacuum than that in previous studies [24, 25].

The paper is organized as follows. In Sec. II, we describe the quantum Rabi model in the presence of a frequency modulation of the quantum two-level system. In Secs. III and IV, we present approaches to enhance and suppress the CR interactions in the JC regime and the ultrastrong-coupling regime, respectively. We also study the bosonic excitation emission from bosonic vacuum in the enhancement case by calculating the output bosonic excitation flux rate. We present some analyses on the implementation of this scheme with circuit-QED systems in Sec. V. Discussions and conclusions are given in Sec. VI.

## II. THE SYSTEM AND HAMILTONIAN

We consider the quantum Rabi model, which contains a quantum two-level system interacting with a bosonic field mode (Fig. 1). The Hamiltonian of the Rabi model can be written as ($\hbar = 1$) [1, 2]

$$H_R = H_{\rm JC} + H_{\rm CR}, \tag{1}$$

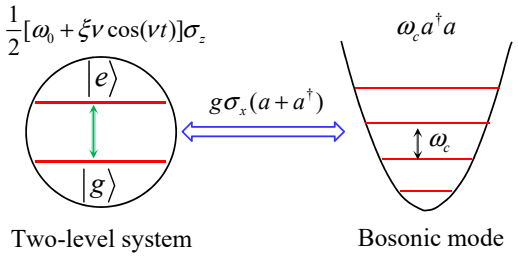


FIG. 1. (Color online) Schematic of the modulated quantum Rabi model. A quantum two-level system with an energy separation $\omega_0$ between its excited state $|e\rangle$ and ground state $|g\rangle$ is coupled to a bosonic field mode with resonance frequency $\omega_c$. The coupling between the two-level system and the bosonic mode has the form $g\sigma_x(a+a^\dagger)$. The energy separation of the two-level system is modulated with a term $(1/2)\xi\nu\cos(\nu t)\sigma_z$.

where

$$H_{\rm JC} = \omega_c a^\dagger a + \frac{\omega_0}{2}\sigma_z + g(\sigma_+ a + a^\dagger \sigma_-), \tag{2}$$

is the usual JC Hamiltonian, and

$$H_{\rm CR} = g(\sigma_- a + a^\dagger \sigma_+), \tag{3}$$

includes the CR terms. Here, $a$ ($a^\dagger$) is the annihilation (creation) operator of the bosonic mode with frequency $\omega_c$. The quantum two-level system is described by the Pauli operator $\sigma_z = |e\rangle\langle e| - |g\rangle\langle g|$ and the transition operators $\sigma_+ = \sigma_-^\dagger = |e\rangle\langle g|$, where $|e\rangle$ and $|g\rangle$ are the excited state and the ground state, respectively, with an energy separation $\omega_0$. The $g$ terms in $H_R$ describe the interactions between the two-level system and the bosonic mode. It should be pointed out that our model is general and system-independent, and it can be implemented with various experimental setups.

To manipulate the CR terms in the Rabi interactions, we introduce a sinusoidal modulation to the energy separation of the two-level system. The modulation Hamiltonian is given by

$$H_M(t) = \frac{1}{2}\xi\nu\cos(\nu t)\sigma_z, \tag{4}$$

where $\nu$ and $\xi$ are the modulation frequency and normalized modulation amplitude, respectively. We note that frequency modulation has been recently studied in various tasks in quantum optics [39–46]. The total Hamiltonian of this system under the frequency modulation is then $H(t) = H_R + H_M(t)$, which can be divided as the following:

$$H(t) = H_0(t) + H_I, \tag{5}$$

with

$$H_0(t) = \omega_c a^\dagger a + \frac{1}{2}[\omega_0 + \xi\nu\cos(\nu t)]\sigma_z, \tag{6a}$$

$$H_I = g\sigma_x(a + a^\dagger). \tag{6b}$$

Here $H_0(t)$ is the time-dependent non-interacting Hamiltonian of the two-level system and the bosonic mode, and $H_I$ describes the coupling between the two subsystems. It should be noted that the $z$-direction modulation in $H_0(t)$ will lead to some interesting physics in this system. When the interaction between the two-level system and the bosonic mode is absence, the modulation sinusoidally changes the eigen-energy of the two-level system. In this case, the change of the internal energy in the two-level system is caused by the work done on the system by the driving source, and there is no heat exchange between the system and the driving source because the population of the two states does not change [47]. Differently, in the presence of the coupling term $H_I$, the time modulation of the Hamiltonian $H_0(t)$ produces sidebands in the spectrum of the two-level system, e.g., the two-level system spectrum now includes $\omega_0 \pm n\nu$, with $n$ being an integer. Such sidebands correspond to injection and extraction of the $n$ bosonic excitations at frequency $\nu$ to the coupled system.

To study the impact of the frequency modulation on the dynamics of this system, we perform the following transformation on the system

$$V(t) = \mathcal{T}\exp\left[-i\int_0^t H_0(\tau)d\tau\right] = \exp\left\{-i\omega_c t a^\dagger a - i\frac{1}{2}[\omega_0 t + \xi\sin(\nu t)]\sigma_z\right\}, \quad (7)$$

where $\mathcal{T}$ denotes the time-ordering operator. In the rotating frame defined by $V(t)$, the transformed Hamiltonian becomes

$$\begin{aligned}\tilde{H}(t) &= V^\dagger(t)H(t)V(t) - iV^\dagger(t)\dot{V}(t)\\ &= g\left(\sigma_+ e^{i[\omega_0 t+\xi\sin(\nu t)]} + \sigma_- e^{-i[\omega_0 t+\xi\sin(\nu t)]}\right)\\ &\quad\times(ae^{-i\omega_c t} + a^\dagger e^{i\omega_c t})\\ &= \sum_{n=-\infty}^{\infty} gJ_n(\xi)[\sigma_+ a e^{i(\delta+n\nu)t} + \text{H.c.}]\\ &\quad + \sum_{m=-\infty}^{\infty} gJ_m(\xi)[\sigma_+ a^\dagger e^{i\Delta_m t} + \text{H.c.}], \end{aligned} \quad (8)$$

where $\delta = \omega_0 - \omega_c$ is the detuning between the unmodulated two-level system and the bosonic mode, $J_n(\xi)$ is the $n$th Bessel function of the first kind, and

$$\Delta_m = \omega_0 + \omega_c + m\nu \quad (9)$$

are the oscillating frequencies of the CR terms. In the derivation of $\tilde{H}(t)$, we have used the Jacobi-Anger expansion,

$$e^{i\xi\sin(\nu t)} = \sum_{n=-\infty}^{\infty} J_n(\xi)e^{in\nu t}. \quad (10)$$

The rotating and CR terms in Hamiltonian $\tilde{H}(t)$ can be tailored by choosing appropriate modulation parameters $\xi$ and $\nu$. For the rotating terms (the fourth line)

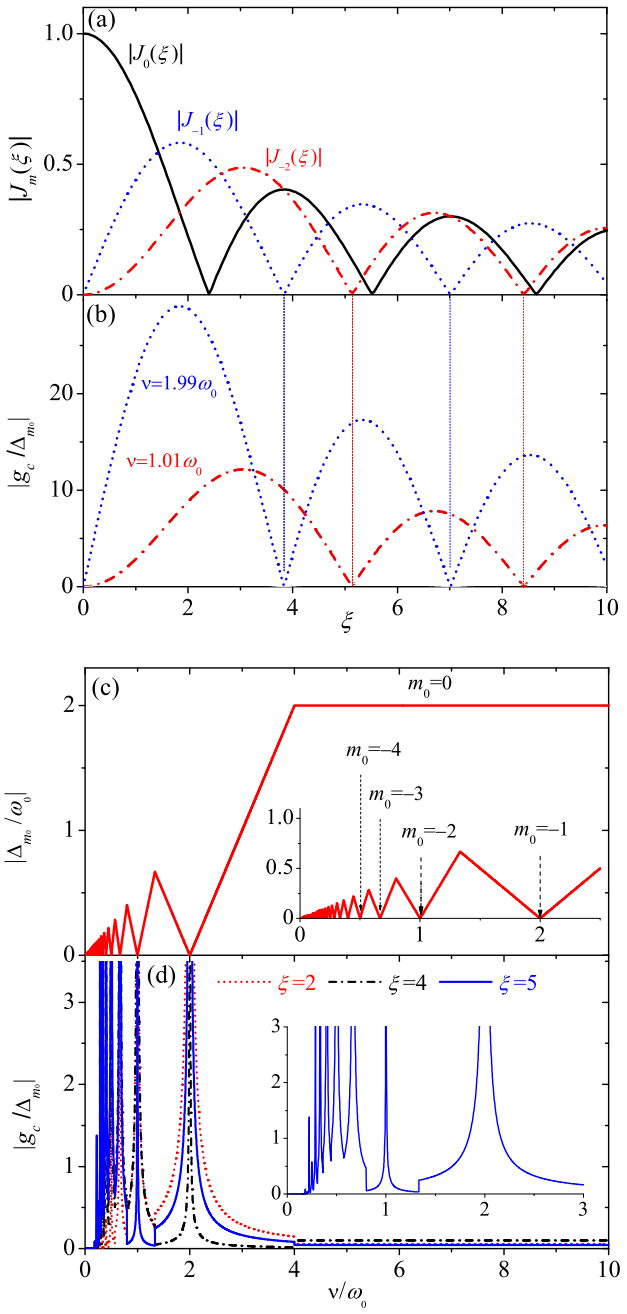


FIG. 2. (Color online) Plots of the absolute value of the Bessel function of the first kind $|J_m(\xi)|$, and the ratios $|g_c/\Delta_{m_0}|$ and $|\Delta_{m_0}/\omega_0|$ versus the normalized modulation amplitude $\xi$ and the scaled modulation frequency $\nu/\omega_0$. (a) Plot of $|J_m(\xi)|$ as a function of $\xi$ at $m = 0$, $-1$, and $-2$. (b) Dependence of $|g_c/\Delta_{m_0}|$ on $\xi$ at $\nu = 1.01\omega_0$ and $1.99\omega_0$. (c) The ratio $|\Delta_{m_0}/\omega_0|$ as a function of $\nu/\omega_0$. (d) The ratio $|g_c/\Delta_{m_0}|$ versus $\nu/\omega_0$ at $\xi = 2$, 4, and 5. The insets in panels (c) and (d) show the detail of the curves for smaller values of $\nu/\omega_0$. Other parameters are given by $g = 0.5\omega_0$ and $\omega_c = \omega_0$.

in Eq. (8), the detunings of the sidebands $(\delta + n\nu)$ are separated from each other by $(n - n')\nu$ with $n$, $n'$ being integers. Under the condition $\nu \gg g > g|J_n(\xi)|$, all the rotating terms other than the 0th-order sideband with the effective coupling strength $gJ_0(\xi)$ can be discarded using the RWA. For the CR terms, there exists a CR sideband $m = m_0$ that satisfies

$$|\Delta_{m_0}| = \min\{|\Delta_m| = |\omega_0 + \omega_c + m\nu|, m \in Z\}, \quad (11)$$

where "$Z$" denotes the set of all integers. The detunings of all other CR sidebands are $\Delta_{m_0+s} = \Delta_{m_0} + s\nu$, with $s$ being a nonzero integer. Under the conditions

$$\nu \gg |\Delta_{m_0}|, \quad \nu \gg g > g|J_m(\xi)|, \quad (12)$$

all the other CR terms can be discarded with the RWA. The Hamiltonian $\tilde{H}(t)$ can hence be approximated as

$$\tilde{H}_1(t) \approx (g_r\sigma_+ a e^{i\delta t} + g_c\sigma_+ a^\dagger e^{i\Delta_{m_0}t}) + \text{H.c.}, \quad (13)$$

where we introduce the normalized coupling strengths

$$g_r = gJ_0(\xi), \qquad g_c = gJ_{m_0}(\xi) \quad (14)$$

for the near resonant rotating and CR terms, respectively. The Hamiltonian (13) describes an effective isotropic Rabi model with $g_r = g_c$ or an effective anisotropic Rabi model with $g_r \neq g_c$ [49] with an effective bosonic mode frequency $\tilde{\omega}_c = (\Delta_{m_0} - \delta)/2$ and an effective frequency $\tilde{\omega}_0 = (\Delta_{m_0} + \delta)/2$ for the quantum two-level system. On one side, we can choose appropriate $\Delta_{m_0}$ and $\delta$ such that the effective Rabi Hamiltonian $\tilde{H}_1(t)$ enters the ultrastrong-coupling regime with $|g_c|$ reaches 0.1 of the frequencies $\tilde{\omega}_c$ and $\tilde{\omega}_0$. Here, the detuning $\Delta_{m_0}$ can be controlled by adjusting the modulation frequency $\nu$. On the other side, the normalized coupling strengths $g_r$ and $g_c$ can be varied in a large range by tuning $\xi$.

To show how to control the interactions between the two-level system and the bosonic field, in Fig. 2 we plot the absolute value of the Bessel function of the first kind $|J_m(\xi)|$, $|\Delta_{m_0}|$, and the ratio $|g_c/\Delta_{m_0}|$ versus the normalized modulation amplitude $\xi$ and the modulation frequency $\nu$, respectively. In panel 2(a), we show $|J_{m=0,-1,-2}(\xi)|$ as a function of $\xi$. We can see that the interaction strengths $g_r$ and $g_c$ can be controlled by choosing a proper work value of $\xi$, as expected by Eq. (14). One can choose a value of $\xi$ satisfying $J_0(\xi) = 0$ (the zero points of the Bessel function) such that the $g_r$ term in Eq. (13) disappears and then a pure CR interaction term is achieved. The effect of the CR interaction is determined by the ratio $|g_c/\Delta_{m_0}|$, as shown in panel 2(b) for a given $\nu$ and in panel 2(d) for a given $\xi$. We observe that the value of $|g_c/\Delta_{m_0}|$ ranges from 0 to $\infty$. The zero points of $|g_c/\Delta_{m_0}|$ correspond to the zero points of $J_{m_0}(\xi)$, as shown in panels. 2(a) and 2(b). The values $\nu/\omega_0 = 1.99$ and 1.01 used in panel 2(b) correspond to the Bessel function $m_0 = -1$ and $-2$ in panel 2(a), respectively. The divergence of $|g_c/\Delta_{m_0}|$ corresponds to the resonance condition $\Delta_{m_0} = 0$, which located at

$$\nu = -\frac{\omega_0 + \omega_c}{m_0}, \quad (15)$$

as shown in panel 2(c). Panel 2(c) shows the dependence of $|\Delta_{m_0}|$ on $\nu$. We can tune the modulation frequency $\nu$ such that a desired sideband characterized by $m_0$ dominates the CR interactions. The v-shaped valley containing a given zero point shares the same $m_0$, and these peaks (i.e., the boundary point of the $m_0$ and $m_0 - 1$ valleys) are located at $2(\omega_0 + \omega_c)/(2|m_0| + 1)$. We can choose proper value of $\xi$ and $\nu$, such that the effect of CR interaction terms can be manipulated. To suppress the CR interaction terms, a large $\nu$ should be chosen such that the ratio $|g_c/\Delta_m|$ is very small and thus the rotating terms dominate the interactions, as shown in the right part of panel 2(d). To enhance the CR interaction terms, the ratio $|g_c/\Delta_m|$ should be increased, which is accessible around resonance $\Delta_{m_0} = 0$, indicated by Eq. (15).

## III. ENHANCEMENT OF THE CR TERMS

In this section, we study the enhancement of the CR terms in the JC regime, where, roughly speaking, $g < 0.1\omega_0$, $0.1\omega_c$. In this regime and under the near-resonance condition $|\delta| \ll \omega_0$, $\omega_c$, the CR interactions $H_{\text{CR}}$ in the Rabi Hamiltonian $H_R$ can be safely omitted by applying the RWA, and $H_R$ is then reduced to the JC Hamiltonian $H_{\text{JC}}$. However, by virtues of the modulation, when the detuning $|\Delta_{m_0}|$ is comparable to or much smaller than $|g_c|$, i.e., $|\Delta_{m_0}| \ll |g_c|$, the CR terms can be strongly enhanced. Then the system is governed by the effective Rabi Hamiltonian (13). Moreover, the condition $|\Delta_{m_0}| \ll |g_c|$ is achievable as shown in Fig. 2. An interesting case is the resonant CR interaction at $\Delta_{m_0} = 0$ at selected value of $m_0$ with $m_0$ being a negative integer. This indicates that the modulated CR interactions can be enhanced even though they are negligibly weak in the original representation. In this section, we will restrict ourself in the condition $|\Delta_{m_0}| \ll |g_c|$ to show how to enhance the CR interactions by introducing frequency modulation to the two-level system and evaluate the validity by calculating the fidelity.

### A. Fidelity and dynamics

We first evaluate the validity of the RWA in deriving the effective Rabi Hamiltonian (13), which can be checked by studying the fidelity

$$F(t) = |\langle\phi(t)|\psi(t)\rangle|^2 \quad (16)$$

between the state $|\phi(t)\rangle$ obtained by solving the Schrödinger equations with the exact Hamiltonian (8) and the state $|\psi(t)\rangle$, obtained by the effective Hamiltonian (13). Here, we choose an initial state $|\phi(0)\rangle = |\psi(0)\rangle = (1/\sqrt{2})(|g\rangle + |e\rangle)|\alpha\rangle$, where $|\alpha\rangle$ is a coherent state of the bosonic mode, to calculate the fidelity.

In Fig. 3(a), we plot the fidelity $F(t)$ as a function of time for several values of the modulation frequency

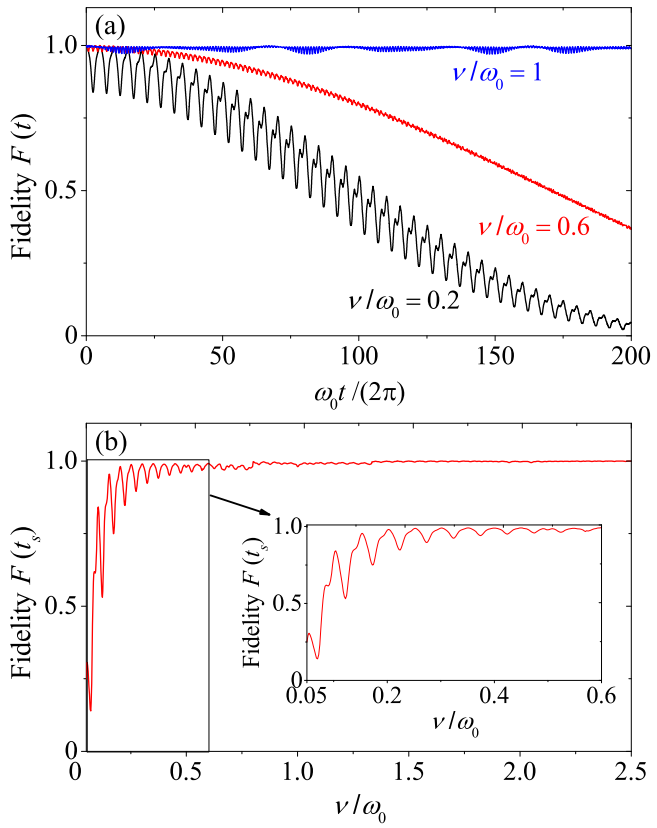


FIG. 3. (Color online) (a) Fidelity $F(t)$ defined in Eq. (16) versus the time for various values of the modulation frequency: $\nu = 0.2\omega_0 = 4g$ (black solid curve), $\nu = 0.6\omega_0 = 12g$ (red solid curve), and $\nu = \omega_0 = 20g$ (blue solid curve). (b) Fidelity $F(t_s)$ at time $t_s = 2\pi/g$ as a function of $\nu$. Other parameters are $\xi = 2.40483$, $\omega_c = \omega_0$, and $g = 0.05\omega_0$. The initial state of the system is $(1/\sqrt{2})(|g\rangle + |e\rangle)|\alpha\rangle$, where $|\alpha\rangle$ is a coherent state with $\alpha = 0.1$.

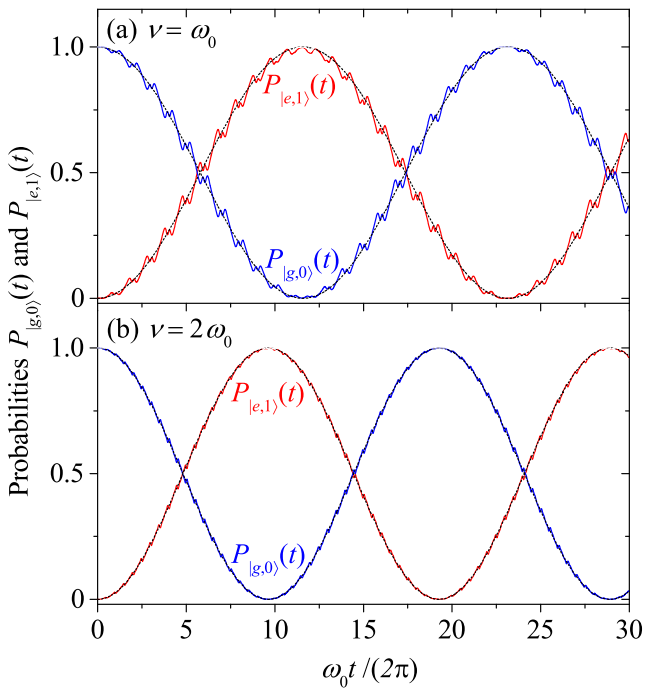


FIG. 4. (Color online) Time dependence of the probabilities $P_{|g,0\rangle}(t)$ (blue solid curves) and $P_{|e,1\rangle}(t)$ (red solid curves) obtained by the exact Hamiltonian $\tilde{H}(t)$ when the modulation frequency $\nu$ satisfies sideband resonance condition at two different values: (a) $\nu = \omega_0$ ($m_0 = -2$), (b) $\nu = 2\omega_0$ ($m_0 = -1$). The black short-dashed curves are the analytical results in Eq. (18) obtained by the effective Hamiltonian $\tilde{H}_{\rm aJC}(t)$. Other parameters are $J_0(\xi) = 0$ ($\xi = 2.40483$), $g = 0.05\omega_0$, and $\omega_c = \omega_0$. The initial state of the system is $|g, 0\rangle$.

$\nu$ starting from the initial state $|\phi(0)\rangle$. Here, for a given $\nu$, the sideband integer $m_0$ is chosen such that the corresponding CR term is the most resonant term, i.e., $m_0 = \texttt{Round}[-(\omega_0 + \omega_c)/\nu]$, where $\texttt{Round}[x]$ is a function for getting the nearest integer of $x$. Figure 3(a) shows that the fidelity experiences oscillations with time. When $\nu$ is much smaller than $\omega_0$, such as $\nu = 0.2\omega_0 = 4g$, the envelope of the fidelity decreases with time accompanied by periodic revival in a long range of time. For larger $\nu$, better fidelity can be obtained, which is in accordance with conditions (12). To find out how the fidelity depends on the frequency $\nu$, in Fig. 3(b), we plot the fidelity $F(t_s)$ at time $t_s = 2\pi/g$ as a function of $\nu$. We see that the fidelity at $t_s$ experiences a fast oscillation for $\nu/\omega_0 < 0.8$. However, the envelope of the fidelity increases gradually with the modulation frequency $\nu$. For $\nu > \omega_0 = 20g$, a high fidelity $[F(t_s) \approx 1]$ can be obtained.

The above technique can be used to produce pure CR interactions. By choosing proper values of $\xi$, the rotating terms in Eq. (13) disappear. For example, at $\xi = 2.40483$, $J_0(\xi) = 0$, and the Hamiltonian (13) becomes

$$\tilde{H}_{\rm aJC}(t) \equiv g_c(\sigma_+ a^\dagger e^{i\Delta_{m_0}t} + a\sigma_- e^{-i\Delta_{m_0}t}), \tag{17}$$

which only contains the CR terms. An essential feature associated with this Hamiltonian is the Rabi oscillation between the states $|g, 0\rangle$ and $|e, 1\rangle$, where $|n = 0, 1\rangle$ are number states of the bosonic mode. Note that multiphoton Rabi oscillations in ultrastrongly-coupled cavity-QED systems have recently been considered [36]. With $\tilde{H}_{\rm aJC}(t)$ and the initial state $|g, 0\rangle$, the probabilities of the system in states $|g, 0\rangle$ and $|e, 1\rangle$ can be obtained as

$$P_{|g,0\rangle}(t) = \frac{4g_c^2}{4g_c^2 + \Delta_{m_0}^2} \cos^2\left(\frac{1}{2}\sqrt{4g_c^2 + \Delta_{m_0}^2}\, t\right), \tag{18a}$$

$$P_{|e,1\rangle}(t) = \frac{4g_c^2}{4g_c^2 + \Delta_{m_0}^2} \sin^2\left(\frac{1}{2}\sqrt{4g_c^2 + \Delta_{m_0}^2}\, t\right). \tag{18b}$$

This Rabi oscillation can be utilized to evaluate the validity of the RWA performed in this modulation scheme. To this end, we compare the exact dynamics of the system governed by the exact Hamiltonian (8) with the analytical solution in Eq. (18).

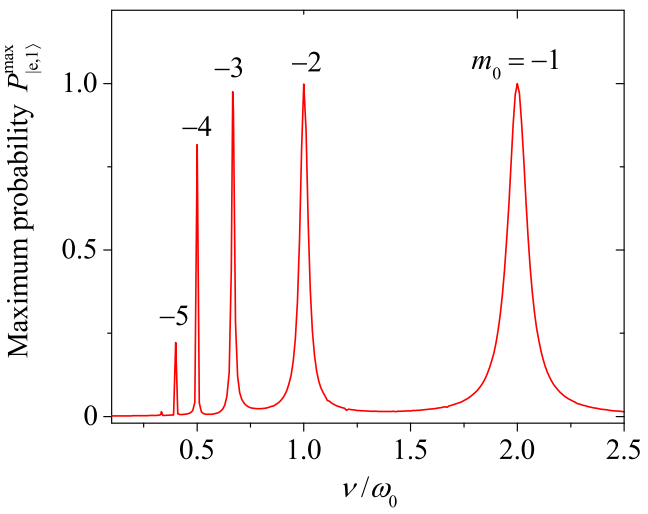


FIG. 5. (Color online) Maximum probability $P^{\max}_{|e,1\rangle}$ of state $|e,1\rangle$ versus the modulation frequency $\nu$. Other parameters are the same as those in Fig. 4.

In Fig. 4, we show the exact and approximate results at two different resonance sidebands, i.e., different values of $m_0$ under $\Delta_{m_0} = 0$. Figures 4(a) and 4(b) correspond to $m_0 = -2$ and $-1$, respectively. Figure 4 shows that the approximate result agrees well with the exact dynamics when the conditions (12) are satisfied. The system demonstrates a clear Rabi oscillation (with period $\pi/|g_c|$) between the states $|g,0\rangle$ and $|e,1\rangle$, and the leakage of the system out of this subspace (spanned by $|g,0\rangle$ and $|e,1\rangle$) is negligible. These features are evidences of the validity of the RWA, and clearly show the enhancement of CR interactions under well-designed frequency modulation. In the absence of modulation (when $H_M = 0$), the system will stay in the state $|g,0\rangle$, which is the ground state of the Hamiltonian $H_R$ under the RWA.

The above sideband-resonance effect can be illustrated more clearly by studying the dependence of the maximum probability $P^{\max}_{|e,1\rangle}$ on the modulation frequency $\nu$. As we sweep the modulation frequency $\nu$, there exist a sequence of resonance windows which correspond to different values of $m_0$ when the resonance condition (15) ($\Delta_{m_0} = 0$) is satisfied. At resonance, the effective Hamiltonian becomes (17) by applying the RWA with the conditions (12) and $J_0(\xi) = 0$. In this case, the maximum probability of state $|e,1\rangle$ in the Rabi oscillation can be obtained. In Fig. 5, we plot the exact maximum probability $P^{\max}_{|e,1\rangle}$ as a function of $\nu$ with the same parameters as those used in Fig. 4. We see from Fig. 5 that there are resonance peaks at locations predicted by Eq. (15).

The linewidths of the resonance peaks in Fig. 5 can be obtained by analyzing the resonance condition. At exact resonance with $\Delta_{m_0} = 0$, the maximum value of the probability is almost one: $P^{\max}_{|e,1\rangle} \approx 1$. According to Eq. (18), with the increase of the detuning $|\Delta_{m_0}|$, the value of $P^{\max}_{|e,1\rangle}$ decreases approximately by the relation $4g_c^2/(4g_c^2+\Delta_{m_0}^2)$, which is a Lorentzian function of $|\Delta_{m_0}|$. Therefore, the line widths of these peaks are determined by the full width at half maximum, i.e., $|\Delta_{m_0}/(2g_c)| \approx 1$. A rough estimation gives the line width for the peak associated with $m_0$ as $|2gJ_{m_0}(\xi)/m_0|$ at $\xi = 2.40483$, which decreases with the increase of $|m_0|$, in accordance with Fig. 5. In addition, Fig. 5 shows that the height of the two peaks ($m_0 = -5, -4$) from the left is smaller than one. This is because there exist some rotating terms which will affect the population significantly. For example, when $m_0 = -4$, the rotating and CR terms at $m = -2$ have a considerable effect on the dynamics. It is worth noting that the present mechanism of enhancing the CR interactions works well for other values of detuning $\delta$. This is because the resonance condition $\Delta_{m_0} = 0$ is independent of the detuning $\delta$.

### B. Output bosonic excitation flux

The above discussions are valid for a closed system without dissipation. In this section, we study the impact of the frequency modulation in the presence of environmental noise, namely, how the modulation affects the system transitions induced by the environment. We assume that the two-level system and the bosonic mode are each connected to a (different) zero-temperature bath. In the absence of the modulation, the system is well described by the JC model. When the system is initially prepared in its ground state $|g,0\rangle$, the system will always stay in this state under a zero-temperature bath and there is no output excitation flux emitted from the bosonic mode. When an appropriate modulation is applied, the system is described by the quantum Rabi model. In this case, though the system is initially prepared in the state $|g,0\rangle$, the dissipation induced by the zero-temperature baths will lead to a finite excitation flux to the continuous modes coupled to bosonic mode (the output excitations will be emitted photons for cavity-QED systems). This is because the state $|g,0\rangle$ is not a ground state of the Rabi model; instead, it is a superposition of many eigenstates of this model. The dissipation will induce transitions from upper eigenstates to lower eigenstates, and the bosonic mode will then emit excitations.

To verify the above analyses, we simulate the bosonic excitation emission in the open-system case under the frequency modulation. In this case, the evolution of the system is governed by the quantum master equation [22, 24, 25]

$$\frac{d\rho(t)}{dt} = i[\rho(t), H(t)] + \sum_{s=a,c}\sum_{k>j}\sum_{j=1}^{\infty}\Gamma_{kj}^{(s)}\{D[|\varepsilon_j\rangle\langle\varepsilon_k|]\rho(t)\}, \quad (19)$$

where $\rho(t)$ is the density matrix of the system in the Schrödinger picture, $H(t)$ is the Hamiltonian of the system given by Eq. (5), and $D[|\varepsilon_j\rangle\langle\varepsilon_k|]$ is a standard Lind-

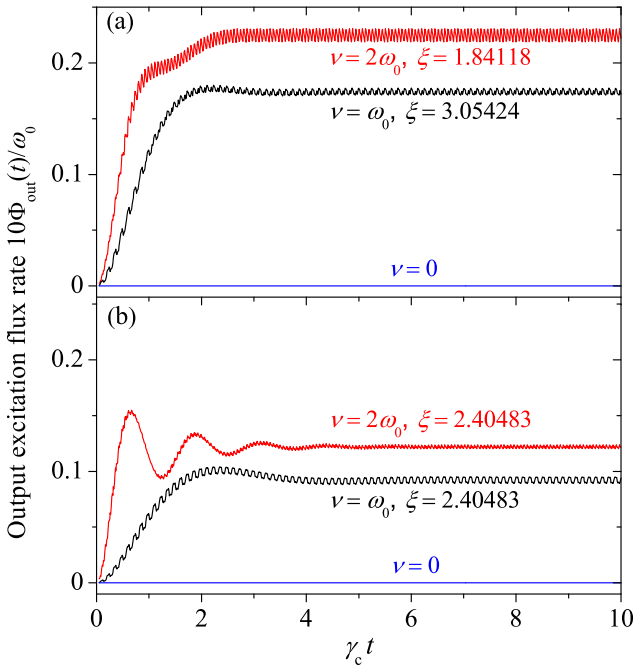


FIG. 6. (Color online) Time dependence of the output bosonic excitation flux rate $\Phi_{\rm out}(t)$ in various cases with resonant CR interactions ($\Delta_{m_0} = 0$) but different coupling strengths $g_r$ and $g_c$. Corresponding to $\nu = \omega_0$ ($2\omega_0$), the sideband parameter of the resonant term is $m_0 = -2$ ($-1$). (a) The parameter $\xi$ is chosen such that the coupling strength $|g_c| = g|J_{m_0}(\xi)|$ corresponding to the resonant $m_0$ term is maximized. (b) The parameter $\xi = 2.40483$ is chosen such that the rotating terms in Eq. (13) disappears [$J_0(\xi) = 0$] and the Hamiltonian is given by Eq. (17). In these two panels, the unmodulated case $\nu = 0$ is presented for comparison. Other parameters are $\delta = 0$, $g = 0.05\omega_0$, and $\gamma_a = \gamma_c = 0.02\omega_0$. The initial state of the system is $|g, 0\rangle$.

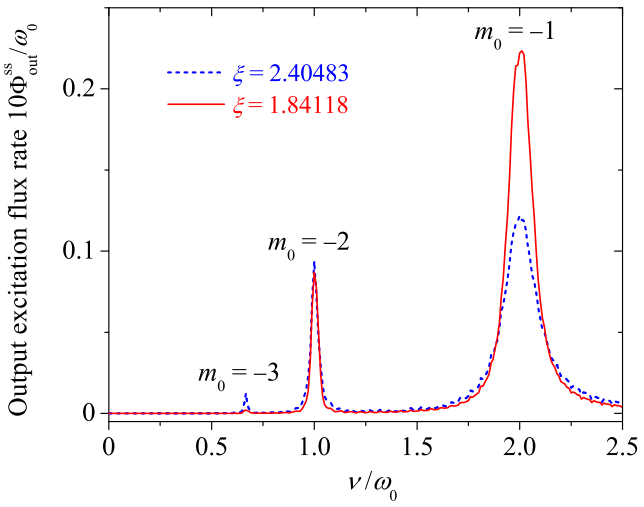


FIG. 7. (Color online) Steady-state output excitation flux rate $\Phi^{\rm ss}_{\rm out}$ versus the modulation frequency $\nu$ for $\xi = 1.84118$ and $\xi = 2.40483$. Other parameters are $\delta = 0$, $g = 0.05\omega_0$, and $\gamma_a = \gamma_c = 0.02\omega_0$. The initial state of the system is $|g, 0\rangle$.

blad superoperator defined by

$$D[O]\rho = O\rho O^\dagger - \frac{1}{2}O^\dagger O\rho - \frac{1}{2}\rho O^\dagger O, \tag{20}$$

with $|\varepsilon_j\rangle\langle\varepsilon_k|$ being state transition operators among the eigenstates of the Rabi Hamiltonian: $H_R|\varepsilon_n\rangle = \varepsilon_n|\varepsilon_n\rangle$ for $n = 1, 2, 3, \cdots$. The relaxation coefficients in Eq. (19) are given by

$$\Gamma_{kj}^{(s=a,c)} = \gamma_s |C_{jk}^{(s)}|^2, \tag{21}$$

where $\gamma_a$ and $\gamma_c$ are the decay rates of the two-level system and the bosonic mode, respectively, and $C_{jk}^{(s=a,c)}$ are the matrix elements of the operators $\sigma_x$ and $(a + a^\dagger)$ in the eigen-representation of the Rabi model. These matrix elements are given by

$$C_{jk}^{(a)} = \langle\varepsilon_j|\sigma_x|\varepsilon_k\rangle, \tag{22a}$$

$$C_{jk}^{(c)} = \langle\varepsilon_j|(a + a^\dagger)|\varepsilon_k\rangle. \tag{22b}$$

In the open-system case, the system will transit from upper eigenstates to lower eigenstates and excitations will be released from the bosonic mode. The output excitation flux can be calculated in terms of the input-output relation. In the ultrastrong-coupling regime, the input-output relation is defined by [22, 24, 25]

$$B_{\rm out}(t) = B_{\rm in}(t) - i\sqrt{\gamma_c}X_c(t), \tag{23}$$

where $B_{\rm in}(t)$ and $B_{\rm out}(t)$ are, respectively, the input and output operators, and $X_c(t)$ is the lowering operator in the Heisenberg picture.

In the absence of external bosonic driving, the output excitation flux rate can be obtained as [24, 25]

$$\Phi_{\rm out}(t) = \langle B_{\rm out}^\dagger(t)B_{\rm out}(t)\rangle = \gamma_c {\rm Tr}[\rho(t)X_c^\dagger X_c], \tag{24}$$

where

$$X_c = \sum_{k>j}\sum_{j=1}^{\infty} C_{jk}^{(c)}|\varepsilon_j\rangle\langle\varepsilon_k| \tag{25}$$

is the lowering operator in the Schrödinger picture.

In Fig. 6, we plot the time dependence of the output bosonic excitation flux rate $\Phi_{\rm out}(t)$ when the CR interaction in Eq. (13) is at resonance. For $\nu = \omega_0$ ($2\omega_0$), the sideband parameter of the resonant term is $m_0 = -2$ ($-1$). We also present the result of the unmodulated case $\nu = 0$ for comparison. In Fig. 6(a), the parameter $\xi$ is chosen such that the coupling strength $g_c$ in the corresponding resonant CR terms can be maximized. Namely, a maximum value of $J_{m_0}(\xi)$ is reached. When $\nu = 2\omega_0$, the $m_0 = -1$ term becomes resonant by $\Delta_{m_0} = 0$, and we choose $\xi = 1.84118$ to obtain a maximum value of $|J_{-1}(1.84118)| = 0.581865$. Similarly, when $\nu = \omega_0$, the $m_0 = -2$ term becomes resonant, and we let $\xi = 3.05424$ to maximize $|J_{-2}(3.05424)| = 0.486499$. From Fig. 6(a) we see that the output bosonic excitation

flux rate increases gradually with the increase of time. When $t \gg \pi/\gamma_c$, the value of $\Phi_{\rm out}(t)$ approaches a stationary value with a small oscillation, which is caused by the discarded terms under the RWA. A nonzero stationary value of $\Phi_{\rm out}(t)$ implies a continuous emission of real excitation from the bosonic vacuum in the stationary state. However, no real excitation is emitted for the unmodulated case. These results indicate that the enhancement of the CR interactions by the frequency modulation is a key factor in creating real bosonic excitation emission in the JC model.

For the two cases of nonzero $\nu$ in Fig. 6(a), the resonant CR terms are maximized by choosing a proper $\xi$. However, the rotating terms also exist in Hamiltonian (13). To eliminate the rotating terms and obtain pure CR interactions, in Fig. 6(b) we choose the same $\xi$ as used in Fig. 3, $\xi = 2.40483$ [$J_0(\xi) = 0$], such that the rotating terms in Hamiltonian (13) can be neglected. In this case, we can observe similar features as that in Fig. 6(a) in short- and long-time limits. For intermediate time, $\Phi_{\rm out}(t)$ exhibits an oscillatory behavior.

In order to illustrate the dependence of the real bosonic excitation emission on the modulation frequency $\nu$, in Fig. 7, we plot the steady-state output excitation flux rate $\Phi_{\rm out}^{ss}$ as a function of the modulation frequency $\nu$ with the same parameters as used in Fig. 6. Our calculation gives resonance peaks that correspond to sidebands at different $m_0$. The locations of these peaks are determined by the resonance condition $\Delta_{m_0} = 0$, similar to the probability dynamics given in Fig. 5. It is interesting to note that the magnitude of the stationary output bosonic excitation flux rate depends on the coupling strength of the CR interactions. For the $m_0 = -1$ peak ($\nu = 2\omega_0$), the magnitude of the output bosonic excitation flux rate at $\xi = 1.84118$ is larger than the value at $\xi = 2.40483$, because $|J_{-1}(\xi)|$ reaches its maximum at $\xi = 1.84118$.

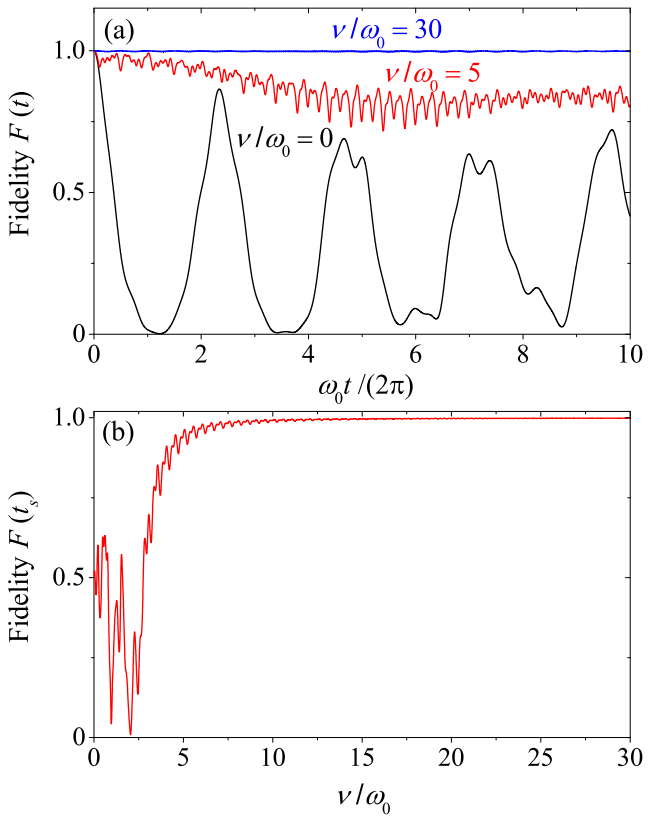


FIG. 8. (Color online) (a) Time dependence of the fidelity $F(t)$ at various values of modulation frequency: $\nu = 0$ (black solid curve), $\nu = 5\omega_0$ (red solid curve), and $\nu = 30\omega_0$ (blue solid curve). (b) Fidelity $F(t_s)$ at time $t_s = 2\pi/g$ as a function of $\nu$. Other parameters are $\xi = 2.21868$ [$J_0(\xi) = 0.1$], $\omega_c = \omega_0$, and $g = 0.5\omega_0$. The initial state of the system is $(1/\sqrt{2})(|g\rangle + |e\rangle)|\alpha\rangle$, where $|\alpha\rangle$ is a coherent state with $\alpha = 0.1$.

## IV. SUPPRESSION OF THE CR TERMS

In this section, we study how to suppress the CR interactions in the ultrastrong-coupling regime by introducing frequency modulation $H_M(t)$ on the quantum two-level system. In the ultrastrong-coupling regime, $g/\omega_0 \geq 0.1$ or $g/\omega_c \geq 0.1$, the CR interactions in $H_{\rm CR}$ become significant. According to our previous analysis, this can be achieved by setting $|\delta| \ll |\Delta_{m_0}|$ and driving the two-level system to reach $|g_c/\Delta_{m_0}| < 0.1$ for $m_0 = 0$. In this scheme, we can adjust the modulation amplitude $\xi$ to reduce $|g_c|$ to well below the ultrastrong coupling limit. At the same time, we choose $\nu$ to satisfy the condition $\nu > 2(\omega_0 + \omega_c)$, which guarantees that $|\Delta_{m_0}| \gg |g_c|$ for $m_0 = 0$ and the contribution from all the $m \neq m_0$ terms is negligible. Note that the reduction of $g_c$ is companied by a reduction of the magnitude of the rotating terms $g_r$. Hence, under the parameter condition

$$\nu \gg \omega_0 + \omega_c \gg \delta, g_c = gJ_{m_0}(\xi), \tag{26}$$

the effective Rabi Hamiltonian (13) can be simplified to a JC Hamiltonian in the interaction-picture

$$\tilde{H}_{\rm JC}(t) \approx g_r(\sigma_+ a e^{i\delta t} + a^\dagger \sigma_- e^{-i\delta t}) \tag{27}$$

with detuning $\delta$ and effective Rabi frequency $g_r$.

To evaluate the validity of the effective Hamiltonian (27), we simulate the dynamics of a quantum state governed by this Hamiltonian. The fidelity of this state in comparison to the exact state generated by Hamiltonian (8), as defined in Eq. (16), is calculated. We choose the initial state as $(1/\sqrt{2})(|g\rangle + |e\rangle)|\alpha\rangle$ ($\alpha = 0.1$), with $|\alpha\rangle$ being a coherent state. In Fig. 8(a), we plot the dynamics of the fidelity $F(t)$ at several values of the modulation frequency $\nu$. We can see that a better fidelity can be obtained for a larger $\nu$, which is in accordance with Eq. (26). In particular, since the coupling strengths of the rotating and the CR terms in Eq. (8) are normalized to $gJ_m(\xi)$ (much smaller than $g$), the RWA performed in obtaining Hamiltonian (27) is valid even under a moderate value of $\nu/\omega_0$ [for example $\nu/\omega_0 = 5$ in Fig. 8(a)].

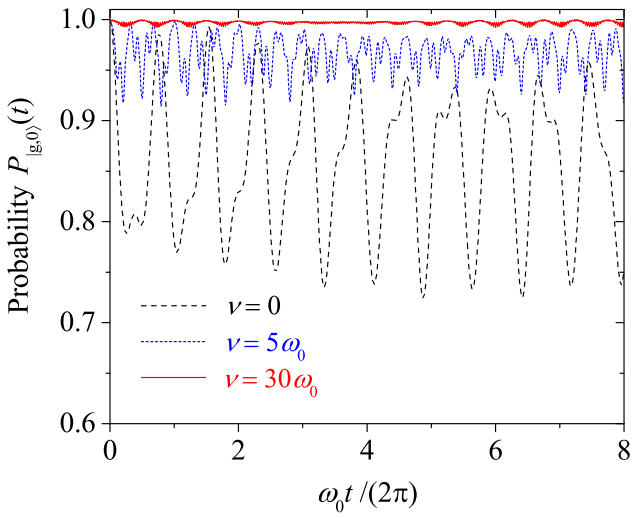


FIG. 9. (Color online) Time dependence of the probability $P_{|g,0\rangle}(t)$ of the system in state $|g,0\rangle$ at various values of $\nu$: $\nu = 0$ (black dashed curve), $\nu = 5\omega_0$ (blue short-dashed curve), and $\nu = 30\omega_0$ (red solid curve). Other parameters are $\xi = 2.21868$ [$J_0(\xi) = 0.1$], $g = 0.5\omega_0$, and $\omega_c = \omega_0$. The initial state of the system is $|g,0\rangle$.

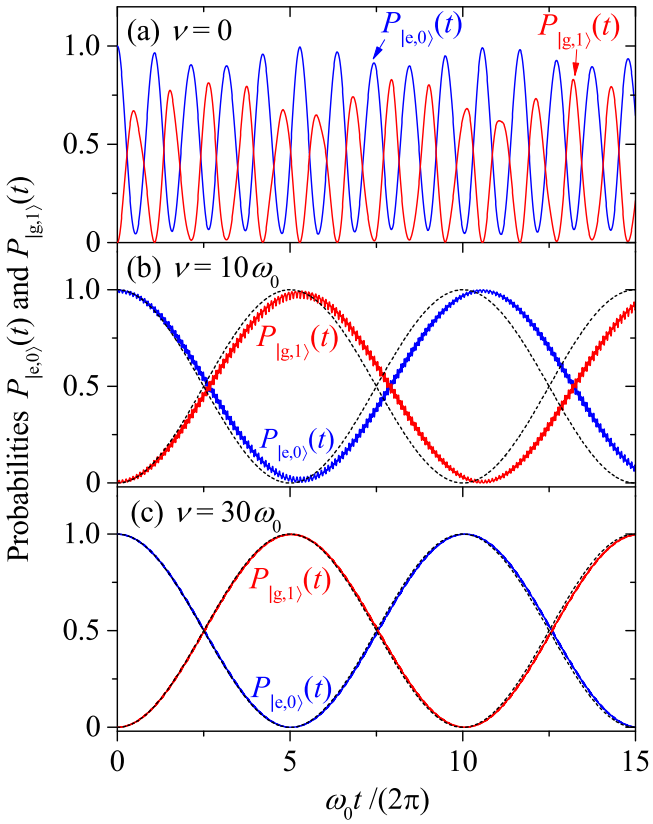


FIG. 10. (Color online) Time dependance of the probabilities $P_{|e,0\rangle}(t)$ (blue solid curves) and $P_{|g,1\rangle}(t)$ (red solid curves) obtained by the exact Hamiltonian (8) at several values of $\nu$: (a) $\nu = 0$, (b) $\nu = 10\omega_0$, and (c) $\nu = 30\omega_0$. The black short-dashed curves in panels (b) and (c) are the Rabi oscillations between the states $|e,0\rangle$ and $|g,1\rangle$ governed by the effective JC Hamiltonian (27). Other parameters are: $g = 0.5\omega_0$, $\xi = 2.21868$ [$J_0(\xi) = 0.1$], and $\omega_c = \omega_0$. The initial state of the system is $|e,0\rangle$.

This is because, for a given discarded term, its contribution is determined by the ratio of the oscillating frequencies over the coupling strength. The larger this ratio, the better the approximation. To investigate how the fidelity depends on the frequency $\nu$ more clearly, in Fig. 8(b), we plot the fidelity $F(t_s)$ at time $t_s = 2\pi/g$ as a function of $\nu$. Figure 8(b) shows that the curve exhibits oscillations followed by a fast increase when $\nu > 2\omega_0$ until reaching a steady value. A high fidelity of $F(t_s) \approx 1$ can be obtained for $\nu > 5\omega_0$.

To illustrate the suppression of the CR terms, in Fig. 9, we plot the probability $P_{|g,0\rangle}(t)$ at various values of the modulation frequency $\nu$ for $\xi = 2.21868$ [$J_0(\xi) = 0.1$ namely $g_r/g = 0.1$] with the system initially prepared in state $|g,0\rangle$. We see that the probability $P_{|g,0\rangle}(t)$ experiences fast oscillations and deviates from 1 significantly in the absence of the modulation. When the modulation is applied, the magnitude of the oscillations decreases gradually with the increase of $\nu$. For sufficiently large $\nu$, the system almost remains in the state $|g,0\rangle$. These features can be understood by analyzing the interactions in the Hamiltonian $\tilde{H}(t)$. When $\nu = 0$, i.e., without the modulation, the system will transit from the state $|g,0\rangle$ to other states with higher number of excitations due to the CR interactions. When the CR interactions are completely suppressed by the modulation, the system is well described by the JC Hamiltonian $\tilde{H}_{\rm JC}(t)$. As a result, the system will stay in the ground state $|g,0\rangle$, which does not evolve under $\tilde{H}_{\rm JC}(t)$.

We also consider the dynamics of this system starting from another initial state $|e,0\rangle$. In Fig. 10, we plot the probabilities $P_{|e,0\rangle}(t)$ and $P_{|g,1\rangle}(t)$ of the states $|e,0\rangle$ and $|g,1\rangle$, respectively, when the modulation frequency $\nu$ takes several values. The solid and short-dashed curves are obtained by using the exact Hamiltonian (8) and the effective Hamiltonian (27), respectively. Figure 10(a) gives the state probabilities of the system in the absence of the modulation. In this case, Hamiltonian (8) reduces to a standard Rabi model in the interaction picture, and the probabilities of states $|e,0\rangle$ and $|g,1\rangle$ experience fast oscillations. More importantly, the total probability $(P_{|e,0\rangle} + P_{|g,1\rangle})$ of the system in the single-excitation subspace spanned by the basis states $|e,0\rangle$ and $|g,1\rangle$ is not normalized to unity due to the transitions induced by the CR terms. However, by introducing a properly-designed modulation under the condition (26), the system can be well characterized by the effective JC Hamiltonian (27). The probabilities ($P_{|e,0\rangle}$ and $P_{|g,1\rangle}$) then become a Rabi oscillation (independent of $\nu$) between the states $|e,0\rangle$ and $|g,1\rangle$, as shown by the black short-dashed curves (approximate probabilities) in Figs. 10(b) and 10(c). In Fig. 10(b), the small deviation of the approximate probabilities from the exact probabilities (solid curves) reflects

the validity of the RWA. However, when the frequency $\nu$ is large enough, for example $\nu/\omega_0 = 30$ [Fig. 10(c)], the exact and approximate probabilities highly overlap with each other. In addition, the periods of the oscillations in Figs. 10(b) and 10(c) are longer than that in Fig. 10(a) due to the modification of the effective Rabi frequency by $J_0(\xi)$.

## V. IMPLEMENTATION WITH A CIRCUIT-QED SETUP

In this section, we present some discussions on the implementation of this scheme with circuit-QED systems. In principle, our modulation approach is general and system-independent, and hence it could be implemented in various Rabi systems possessing both the ultrastrong coupling between the quantum two-level system and the bosonic mode and the longitudinal driving (namely the frequency modulation) on the two-level system, which are two features of the system under consideration. Here, the ultrastrong coupling is needed only for implementation of the suppression case in Sec. IV. For implementation of the enhancement case given in Sec. III, the Rabi interaction should be in the weak or strong-coupling regime. Currently, the ultrastrong-coupling regime has been demonstrated in superconducting circuits [9–13] and semiconductor microcavities [14–16]. Moreover, great advances have been achieved in the manipulation of superconducting qubits (for example, the longitudinal and transverse drivings). Therefore, the mentioned two features of this scheme are accessible in circuit-QED systems. For cavity-QED systems with natural atoms and optical cavities, the weak and strong coupling regimes of the Rabi model have been realized in experiments, and the atomic frequency modulation can also be implemented by introducing proper Stark-shift fields. However, the realization of the ultrastrong coupling in cavity-QED systems is a big challenge. Consequently, to unify discuss the enhancement and suppression schemes in a common system, below we discuss the implementation of this scheme with a circuit-QED system.

The circuit-QED system is formed by a superconducting flux qubit and a lumped-element LC oscillator [12]. The ultrastrong coupling in this system is caused by the mutual inductance between the qubit and the oscillator. In this system, the Hamiltonian of the flux qubit can be written as $H_q = -\varepsilon(t)\tau_z - \Delta(t)\tau_x$ in the basis of two states with persistent currents around the qubit loop, where $\tau_z$ and $\tau_x$ are the Pauli operators in this representation, $\varepsilon$ is the energy separation between the two persistent current states. By choosing a proper magnetic flux threading the qubit loop such that the qubit works at the optimal point, then the parameter $\varepsilon$ disappears. In a four-junction flux qubit, the tunneling splitting $\Delta(t)$ can be tuned independently through the biasing magnetic flux threading the so-called $\alpha$ loop [11, 48]. Furthermore, a driving on the qubit can be introduced by designing proper magnetic fluxes. The coupling induced by the mutual inductance between the qubit and the oscillator can be described by the Hamiltonian $H_I = g\tau_z(a+a^\dagger)$, where $a$ ($a^\dagger$) is the annihilation (creation) operator of the oscillator with frequency $\omega_c$, which is described by the free Hamiltonian $H_o = \omega_c a^\dagger a$. The coupling strength $g$ is proportional to the mutual inductance and the currents in the qubit loop and the LC oscillator. By performing a basis transformation $\{\tau_x \to -\sigma_z, \tau_z \to \sigma_x\}$, the Hamiltonian can be written as $H = \Delta(t)\sigma_z + \omega_c a^\dagger a + g\sigma_x(a^\dagger + a)$. The qubit frequency modulation can be introduced via threading a time-dependent magnetic flux through the $\alpha$ loop. We note that the introduction of qubit modulation with biasing magnetic flux threading the $\alpha$ loop has been proposed to implement quantum information processing in flux qubits [50].

To evaluate the parameter conditions in circuit-QED systems, below we analyze the parameters involved in our scheme. It can be seen from Eqs. (5) and (6) that there are five parameters involved in this model: resonance frequency $\omega_c$ of the bosonic mode, transition frequency $\omega_0$ of the two-level system, Rabi coupling strength $g$, scaled modulation amplitude $\xi$, and modulation frequency $\nu$. In our scheme, $\omega_c = \omega_0$ is considered for the resonant coupling case, and some particular values of the parameter $\xi$ are taken for obtaining desired parametric couplings ($\xi = 2.40483$ and $\xi = 2.21868$ are taken in the enhancement and suppression cases, respectively). As a result, we only need to analyze the values of the two ratios $g/\omega_0$ and $\nu/\omega_0$. In the enhancement case, we choose $g/\omega_0 = 0.05$, and our approach works well when $\nu/\omega_0 \geq 0.5$. In the suppression case, we choose $g/\omega_0 = 0.5$, and the scheme works well (with a fidelity larger than 0.8) when $\nu/\omega_0 \geq 3.5$. Based on the reported experiments [10–12], we know that the resonance frequencies of the qubit and the oscillator can be in the several GHz frequency range, and the coupling strength between the qubit and resonator can be in either the strong- or the ultrastrong-coupling regime (from hundreds of megahertz to some exceed one gigahertz). For example, the ratio $g/\omega_c$ can reach 0.05 - 1.34 in circuit-QED systems [10–12], in accordance with the parameters used in our scheme. The frequency modulation in the qubit Hamiltonian can be implemented by applying proper biasing magnetic fluxes [51–53]. By tuning the driving amplitude and frequency, the modulation parameters $\xi$ and $\nu$ can be chosen on demand. To implement the present scheme, for a suitable modulation frequency $\nu$, the modulation amplitude is determined by $\xi\nu/2$ under a desired value of $\xi$. In circuit-QED systems, the modulation frequency should be in the range from hundreds of megahertz to several gigahertz. As a result, the modulation amplitude should also be approximately in the same range because of $\xi\nu/2 \approx \nu$ for $\xi = 2.40483$ and $\xi = 2.21868$. In realistic experiments, the modulation amplitude was bounded to intermediate values (usually smaller or around one gigahertz) due to the heat effect. Therefore, the enhancement case can be imple-

mented with current experimental condition by choosing the qubit and oscillator frequencies around 2 GHz. To implement the suppression case, however, smaller frequencies of the qubit and the oscillator should be taken for obtaining larger values of $\nu/\omega_0$.

## VI. DISCUSSIONS AND CONCLUSIONS

It deserves to be mentioned that, the physical mechanism of the interaction manipulation in our scheme is the active control of the resonance of involved physical processes. Namely, we choose proper modulation frequency such that the desired physical transitions to be resonant and the undesired transitions to be far-off-resonant. Though we only discussed the quantum regime of the Rabi system, our approach also works in principle for the semiclassical regime, in which a two-level system is coupled to a classical monochromatic field. However, the function of the modulation cannot be recognized from the population of the two-level system in the semiclassical regime. This is because the transitions induced by the rotating and CR terms in the semiclassical regime are the same, i.e. $|g\rangle \leftrightarrow |e\rangle$, hence we do not know how many population is caused by either the rotating terms or the CR terms. This point is different from that in the quantum regime, in which the CR and rotating terms cause different transitions (the system stays in $|g,0\rangle$ or transits from $|g,0\rangle$ to $|e,1\rangle$, corresponding to the rotating and CR interaction terms), hence we can identify the physical process from the transition population of the system. We checked the calculations in the semiclassical regime, and found that the modulation can enhance the CR terms in the non-ultrastrong coupling regime. Meanwhile, in the ultrastrong coupling regime, the modulation can suppress the CR terms and the system experiences a Rabi oscillation at a reduced frequency due to the reduction of the magnitude of the rotating terms.

In conclusion, we have proposed a method to control the CR interactions in the quantum Rabi model by introducing a sinusoidal modulation to the transition frequency of the two-level system. This control scheme includes the enhancement of the CR interactions in the JC regime and the suppression of these terms in the ultrastrong-coupling regime. By designing proper modulation frequency and amplitude, the rotating and CR interactions in the Rabi model can be tailored to be either resonant or far off-resonant. In these cases, we have derived effective Hamiltonians to describe the dynamics of this system and verified detailed parameter conditions under which the approximations are valid. We have also studied the evolution of the state population in this system, which shows clear evidence of the manipulation of the interaction terms. In addition, we have investigated bosonic excitation emission in the enhancement case by calculating the output excitation flux rate. A continuous excitation emission from the bosonic vacuum in the JC regime is obtained.

## ACKNOWLEDGMENTS

One of the authors (J.Q.L.) thanks Prof. Z. H. Peng for helpful discussions on the experimental implementation of this scheme in circuit-QED systems. J.F.H. is supported by the National Natural Science Foundation of China under Grants No. 11447102 and No. 11505055. J.Q.L. is supported in part by National Natural Science Foundation of China under Grant No. 11774087 and Hunan Provincial Natural Science Foundation of China under Grant No. 2017JJ1021. L.T. is supported by the National Science Foundation under Award No. NSF-DMR-0956064. L.M.K. is supported by the National Natural Science Foundation of China under Grants No. 11375060, No. 11434011, and No. 11775075.

[1] I. I. Rabi, On the process of space quantization, Phys. Rev. **49**, 324 (1936).
[2] I. I. Rabi, Space quantization in a gyrating magnetic field, Phys. Rev. **51**, 652 (1937).
[3] E. T. Jaynes and F. W. Cummings, Comparison of quantum and semiclassical radiation theories with application to the beam maser, Proc. IEEE **51**, 89 (1963).
[4] B. W. Shore and P. L. Knight, The Jaynes-Cummings model, J. Mod. Opt. **40**, 1195 (1993).
[5] The weak (strong) coupling regime corresponds to the case in which the coupling strength between the subsystems (two-level system and bosonic mode) is smaller (larger) than their decay rates. In these two cases, the coupling strength should be much smaller than the frequencies of the subsystems to confirm the validity of the RWA.
[6] E. K. Irish, Generalized rotating-wave approximation for arbitrarily large coupling, Phys. Rev. Lett. **99**, 173601 (2007).
[7] C. J. Gan and H. Zheng, Dynamics of a two-level system coupled to a quantum oscillator: transformed rotating-wave approximation, Eur. Phys. J. D **59**, 473 (2010).
[8] D. Braak, Integrability of the Rabi model, Phys. Rev. Lett. **107**, 100401 (2011).
[9] J. Bourassa, J. M. Gambetta, A. A. Abdumalikov, Jr., O. Astafiev, Y. Nakamura, and A. Blais, Ultrastrong coupling regime of cavity QED with phase-biased flux qubits, Phys. Rev. A **80**, 032109 (2009).
[10] T. Niemczyk, F. Deppe, H. Huebl, E. P. Menzel, F. Hocke, M. J. Schwarz, J. J. García-Ripoll, D. Zueco, T. Hümmer, E. Solano, A. Marx, and R. Gross, Circuit quantum electrodynamics in the ultrastrong-coupling regime, Nature Phys. **6**, 772 (2010).
[11] P. Forn-Díaz, J. Lisenfeld, D. Marcos, J. J. García-Ripoll, E. Solano, C. J. P. M. Harmans, and J. E. Mooij, Observation of the Bloch-Siegert shift in a qubit-oscillator system in the ultrastrong coupling regime, Phys. Rev. Lett. **105**, 237001 (2010).

[12] F. Yoshihara, T. Fuse, S. Ashhab, K. Kakuyanagi, S. Saito, and K. Semba, Superconducting qubit-oscillator circuit beyond the ultrastrong-coupling regime, Nature Phys. **13**, 44 (2017) .

[13] P. Forn-Díaz, J. J. García-Ripoll, B. Peropadre, J.-L. Orgiazzi, M. A. Yurtalan, R. Belyansky, C. M. Wilson, and A. Lupascu, Ultrastrong coupling of a single artificial atom to an electromagnetic continuum in the nonperturbative regime, Nature Phys. **13**, 39 (2017).

[14] A. A. Anappara, S. De Liberato, A. Tredicucci, C. Ciuti, G. Biasiol, L. Sorba, and F. Beltram, Signatures of the ultrastrong light-matter coupling regime, Phys. Rev. B **79**, 201303(R) (2009).

[15] G. Günter, A. A. Anappara, J. Hees, A. Sell, G. Biasiol, L. Sorba, S. De Liberato, C. Ciuti, A. Tredicucci, A. Leitenstorfer, and R. Huber, Sub-cycle switch-on of ultrastrong light-matter interaction, Nature (London) **458**, 178 (2009).

[16] Y. Todorov, A. M. Andrews, R. Colombelli, S. De Liberato, C. Ciuti, P. Klang, G. Strasser, and C. Sirtori, Ultrastrong light-matter coupling regime with polariton dots, Phys. Rev. Lett. **105**, 196402 (2010).

[17] A. L. Grimsmo and S. Parkins, Cavity-QED simulation of qubit-oscillator dynamics in the ultrastrong-coupling regime, Phys. Rev. A **87**, 033814 (2013).

[18] D. Ballester, G. Romero, J. J. García-Ripoll, F. Deppe, and E. Solano, Quantum simulation of the ultrastrong-coupling dynamics in circuit quantum electrodynamics, Phys. Rev. X **2**, 021007 (2012).

[19] X. Cao, J. Q. You, H. Zheng, and F. Nori, A qubit strongly coupled to a resonant cavity: asymmetry of the spontaneous emission spectrum beyond the rotating wave approximation, New. J. Phys. **13**, 073002 (2011).

[20] C. K. Law, Vacuum Rabi oscillation induced by virtual photons in the ultrastrong-coupling regime, Phys. Rev. A **87**, 045804 (2013).

[21] S. Ashhab, Superradiance transition in a system with a single qubit and a single oscillator, Phys. Rev. A **87**, 013826 (2013).

[22] A. Ridolfo, M. Leib, S. Savasta, and M. J. Hartmann, Photon blockade in the ultrastrong coupling regime, Phys. Rev. Lett. **109**, 193602 (2012).

[23] A. Ridolfo, S. Savasta, and M. J. Hartmann, Nonclassical radiation from thermal cavities in the ultrastrong coupling regime, Phys. Rev. Lett. **110**, 163601 (2013).

[24] R. Stassi, A. Ridolfo, O. Di Stefano, M. J. Hartmann, and S. Savasta, Spontaneous conversion from virtual to real photons in the ultrastrong-coupling regime, Phys. Rev. Lett. **110**, 243601 (2013).

[25] J. F. Huang and C. K. Law, Photon emission via vacuum-dressed intermediate states under ultrastrong coupling, Phys. Rev. A **89**, 033827 (2014).

[26] S. Felicetti, T. Douce, G. Romero, P. Milman and E. Solano, Parity-dependent State Engineering and Tomography in the ultrastrong coupling regime, Sci. Rep. **5**, 11818 (2015).

[27] Z. Chen, Y. Wang, T. Li, L. Tian, Y. Qiu, K. Inomata, F. Yoshihara, S. Han, F. Nori, J. S. Tsai, and J. Q. You, Single-photon-driven high-order sideband transitions in an ultrastrongly coupled circuit-quantum-electrodynamics system, Phys. Rev. A **96**, 012325 (2017).

[28] J. Casanova, G. Romero, I. Lizuain, J. J. García-Ripoll, and E. Solano, Deep strong coupling regime of the Jaynes-Cummings model, Phys. Rev. Lett. **105**, 263603 (2010).

[29] X. Cao, J. Q. You, H. Zheng, A. G. Kofman, and F. Nori, Dynamics and quantum Zeno effect for a qubit in either a low- or high-frequency bath beyond the rotating-wave approximation, Phys. Rev. A **82**, 022119 (2010).

[30] Q. Ai, Y. Li, H. Zheng, and C. P. Sun, Quantum anti-Zeno effect without rotating wave approximation, Phys. Rev. A **81**, 042116 (2010).

[31] Z. H. Wang, Y. Li, D. L. Zhou, C. P. Sun, and P. Zhang, Single-photon scattering on a strongly dressed atom, Phys. Rev. A **86**, 023824 (2012).

[32] E. Sanchez-Burillo, D. Zueco, J. J. Garcia-Ripoll, and L. Martin-Moreno, Scattering in the ultrastrong regime: nonlinear optics with one photon, Phys. Rev. Lett. **113**, 263604 (2014).

[33] M. O. Scully, Collective Lamb shift in single photon Dicke superradiance, Phys. Rev. Lett. **102**, 143601 (2009).

[34] R. Röhlsberger, K. Schlage, B. Sahoo, S. Couet, and R. Rüffer, Collective Lamb shift in single-photon superradiance, Science **328**, 1248 (2010).

[35] Y. Li, J. Evers, W. Feng, and S. Y. Zhu, Spectrum of collective spontaneous emission beyond the rotating-wave approximation, Phys. Rev. A **87**, 053837 (2013).

[36] L. Garziano, R. Stassi, V. Macrì, A. F. Kockum, S. Savasta, and F. Nori, Multiphoton quantum Rabi oscillations in ultrastrong cavity QED, Phys. Rev. A **92**, 063830 (2015).

[37] J. F. Huang and C. K. Law, Phase-kicked control of counter-rotating interactions in the quantum Rabi model, Phys. Rev. A **91**, 023806 (2015).

[38] S. De Liberato, D. Gerace, I. Carusotto, and C. Ciuti, Extracavity quantum vacuum radiation from a single qubit, Phys. Rev. A **80**, 053810 (2009).

[39] S. N. Shevchenko, S. Ashhab, and F. Nori, Landau-Zener-Stückelberg interferometry, Phys. Rep. **492**, 1 (2010), and references therein.

[40] M. P. Silveri, J. A. Tuorila, E. V. Thuneberg, and G. S. Paraoanu, Quantum systems under frequency modulation, Rep. Prog. Phys. **80**, 056002 (2017), and references therein.

[41] L. Zhou, S. Yang, Y.-x. Liu, C. P. Sun, and F. Nori, Quantum Zeno switch for single-photon coherent transport, Phys. Rev. A **80**, 062109 (2009).

[42] F. Beaudoin, M. P. da Silva, Z, Dutton, and A. Blais, First-order sidebands in circuit QED using qubit frequency modulation, Phys. Rev. A **86**, 022305 (2012).

[43] J. D. Strand, M. Ware, F. Beaudoin, T. A. Ohki, B. R. Johnson, A. Blais, and B. L. T. Plourde, First-order sideband transitions with flux-driven asymmetric transmon qubits, Phys. Rev. B **87**, 220505(R) (2013).

[44] J. Li, M. P. Silveri, K. S. Kumar, J.-M. Pirkkalainen, A. Vepsäläinen, W. C. Chien, J. Tuorila, M. A. Sillanpää, P. J. Hakonen, E. V. Thuneberg, and G. S. Paraoanu, Motional averaging in a superconducting qubit, Nat. Commun. **4**, 1420 (2013).

[45] J.-Q. Liao, C. K. Law, L.-M. Kuang, and F. Nori, Enhancement of mechanical effects of single photons in modulated two-mode optomechanics, Phys. Rev. A **92**, 013822 (2015).

[46] J.-Q. Liao, J.-F. Huang, and L. Tian, Generation of macroscopic Schrödinger-cat states in qubit-oscillator systems, Phys. Rev. A **93**, 033853 (2016).

[47] H. T. Quan, Y.-x. Liu, C. P. Sun, and F. Nori, Quantum thermodynamic cycles and quantum heat engines, Phys.

Rev. E **76**, 031105 (2007).
[48] M. J. Schwarz, J. Goetz, Z. Jiang, T. Niemczyk, F. Deppe, A. Marx, and R. Gross, Gradiometric flux qubits with a tunable gap, New J. Phys. **15**, 045001 (2013).
[49] Q.-T. Xie, S. Cui, J.-P. Cao, L. Amico, and H. Fan, Anisotropic Rabi model, Phys. Rev. X **4**, 021046 (2014).
[50] P.-M. Billangeon, J. S. Tsai, and Y. Nakamura, Circuit-QED-based scalable architectures for quantum information processing with superconducting qubits, Phys. Rev. B **91**, 094517 (2015).
[51] F. G. Paauw, A. Fedorov, C. J. P. M. Harmans, and J. E. Mooij, Tuning the gap of a superconducting flux qubit, Phys. Rev. Lett. **102**, 090501 (2009).
[52] C. Navarrete-Benlloch, J. J. García-Ripoll, and D. Porras, Inducing nonclassical lasing via periodic drivings in circuit quantum electrodynamics, Phys. Rev. Lett. **113**, 193601 (2014).
[53] D. Porras and J. J. García-Ripoll, Shaping an itinerant quantum field into a multimode squeezed vacuum by dissipation, Phys. Rev. Lett. **108**, 043602 (2012).